

The Conducting Ring Viewed as a Wormhole

T Curtright^{1*}, H Alshal^{1,2†}, P Baral¹, S Huang¹, J Liu¹, K Tamang¹, X Zhang¹, and Y Zhang¹

¹Department of Physics, University of Miami, Coral Gables, FL 33124-8046, USA

²Department of Physics, Cairo University, Giza, 12613, Egypt

11 May 2018

Abstract

We compute the exterior Green function for a grounded equi-potential circular ring in two-dimensional electrostatics by treating the system geometrically as a “squashed wormhole” with an image charge located in a novel but obvious position, thereby implementing a method first suggested in 1897 by Sommerfeld. We compare and contrast the strength and location of the image charge in the wormhole picture with that of the conventional point of view where an image charge is located inside the circular ring. While the two viewpoints give mathematically equivalent Green functions, we believe they provide strikingly different physics perspectives. We also comment on earlier Green function results by Hobson in 1900, and by Davis and Reitz in 1971, who applied Sommerfeld’s method to analyze a grounded conducting circular disk in three-dimensional electrostatics.



Richard Feynman (1918-1988) and Arnold Sommerfeld (1868-1951)

*curtright@miami.edu

†alshal@cu.edu.eg

Introduction

Richard Feynman constantly emphasized that insight could be gained by approaching a problem from a different point of view [9]. We follow that philosophy here to construct the Green function “ G_o ” for a grounded circular conducting ring in two-dimensional (2D) electrostatics by stressing the geometrical aspects of a method first employed in the late 19th century by Arnold Sommerfeld [3], albeit not for this specific problem. Although the method was introduced some 120 years ago [11], we believe it suggests insights that are not widely appreciated. Indeed, while Sommerfeld’s method has occasionally been successfully employed during the intervening century to solve a handful of otherwise difficult electrostatic problems [2, 7], we believe that a stronger emphasis on its geometrical aspects is worthwhile and justifies applying the method to a broader class of problems, even those which are not difficult to solve by other means. To that end we reconsider the grounded circular ring.

Although the Green function with homogeneous Dirichlet boundary conditions is well-known for this problem and can be obtained by several methods, here we compute G_o via a novel method that uses “worm-holes” [10, 8] in a 2D Riemannian space. We begin by considering a 2D version of the classic Ellis wormhole [5], whose circular slices have radii given by $r(w) = \sqrt{R^2 + w^2}$ where R is a constant and w is the standard real parameterization of the surface, with $-\infty \leq w \leq +\infty$, constructed so that the region near $w = 0$ is a curved bridge [4] that connects two distinct branches of the surface, with those branches approaching two separate flat planes asymptotically as $w \rightarrow \pm\infty$ (see the Figures).

We build appropriate Green functions for the invariant Laplacian ∇^2 acting on this geometry, initially by imposing boundary conditions only as $w \rightarrow \pm\infty$, to obtain “ G ”, and finally by requiring that the Green function also vanish at $w = 0$, i.e. at radius R , to obtain G_o .

The latter “grounded” Green function G_o is constructed by placing a source and its negative image at exactly the same radius and in precisely the same direction on the surface, but on opposite branches.

Next we introduce a deformation of the Ellis wormhole whose radii are given by the p -norm $r(w) = (R^p + |w|^p)^{1/p}$. We compute Green functions G and G_o for this family of surfaces as well. Finally, we consider the $p \rightarrow 1$ limit of this family of surfaces and Green functions.

In this $p \rightarrow 1$ limit, where $r(w) = R + |w|$ is the so-called Manhattan norm, both branches of the surface are completely “squashed flat”. That is to say, the surface degenerates into two distinct flat planes joined together along the circumference of a circular “doorway”, i.e. a ring of radius R (for views of the surface as p approaches 1, see the Figures). However, the interior of the ring is *excluded* from either plane. Moreover, in this limit it is clear that by restricting G_o to have source and field points on just one of the distinct planes, a Green function for the grounded conducting ring in 2D is obtained. Minor rearrangements of the terms shows that G_o is in exact agreement with the usual symmetrized Green function for the grounded ring, as obtained by considering only *one* Euclidean plane with an image charge placed inside the ring.

Generalizations to several problems in higher dimensions are forthcoming [1].

Electrostatics in two Euclidean dimensions

The point-particle electric potential on the 2D Euclidean plane, \mathbb{E}_2 , is well-known to be logarithmic. For a unit point charge located at the origin, up to a constant R that sets the distance scale,

$$\Phi_{\mathbb{E}_2}(\vec{r}) = -\frac{1}{2\pi} \ln(r/R) , \quad \nabla^2 \Phi_{\mathbb{E}_2}(\vec{r}) = -\delta^2(\vec{r}) , \quad (1)$$

Consequently, a Green function for the plane is

$$G_{\mathbb{E}_2}(\vec{r}_1; \vec{r}_2) = -\frac{1}{2\pi} \ln(|\vec{r}_1 - \vec{r}_2|/R) = -\frac{1}{4\pi} \ln\left(\frac{r_1^2 + r_2^2 - 2r_1 r_2 \cos(\theta_1 - \theta_2)}{R^2}\right) , \quad \nabla^2 G_{\mathbb{E}_2}(\vec{r}_1; \vec{r}_2) = -\delta^2(\vec{r}_1 - \vec{r}_2) \quad (2)$$

This result is translationally invariant on the plane, that is to say, $G_{\mathbb{E}_2}(\vec{r}_1; \vec{r}_2)$ depends only on the difference $\vec{r}_1 - \vec{r}_2$. Moreover, this choice for the Green function incorporates boundary conditions at spatial infinity

that mimic the behavior in (1). So any sufficiently localized¹ charge distribution $\rho(\vec{r})$ on the plane gives rise to the usual linear superposition,

$$\Phi(\vec{r}_1) = \int G_{\mathbb{E}_2}(\vec{r}_1; \vec{r}_2) \rho(\vec{r}_2) d^2r_2 \quad (3)$$

where we assume the integral is well-defined and finite. For a localized charge distribution, $\Phi(\vec{r}_1) \underset{r_1 \rightarrow \infty}{\sim} -\frac{Q}{2\pi} \ln(r_1/R) + O(1/r_1)$ where $Q = \int \rho(\vec{r}_2) d^2r_2$ is the total charge.

Electrostatics in two curved dimensions

On a Riemannian manifold, described by a metric $g_{\mu\nu}$, distance increments are given by ds where

$$(ds)^2 = g_{\mu\nu} dx^\mu dx^\nu \quad (4)$$

Summation over integer μ and ν is implicitly understood, with $1 \leq \mu, \nu \leq N$ for an N -dimensional manifold. The invariant Laplacian on such a manifold is given by

$$\nabla^2 = \frac{1}{\sqrt{g}} \partial_\mu (\sqrt{g} g^{\mu\nu} \partial_\nu) \quad (5)$$

where $g \equiv \det g_{\mu\nu}$ and $g^{\mu\nu}$ is the matrix inverse of $g_{\mu\nu}$, written using the standard “raised index” notation. So, with an implicit sum over μ , we have $g^{\lambda\mu} g_{\mu\nu} = \delta^\lambda_\nu = 1$ if $\lambda = \nu$ but 0 otherwise, i.e. δ^λ_ν is the unit matrix.

Consider now an infinite 2D manifold, e.g. an unbounded surface of revolution embedded in 3D, with

$$(ds)^2 = (dw)^2 + r^2(w) (d\theta)^2 \quad (6)$$

The variables w and θ take on values $-\infty \leq w \leq +\infty$ and $0 \leq \theta \leq 2\pi$, and $r(w)$ is assumed to be a positive, non-vanishing “radius” function that has a minimum at $w = 0$ and becomes infinite as $w \rightarrow \pm\infty$. For a fixed angle, radial displacements on the manifold are determined just by $ds = \pm dw$.

We refer to $w > 0$ and $w < 0$ respectively as the “upper” and “lower” branches of the manifold, and we call the region near $w = 0$ the “bridge” between the two branches. For visualization purposes, see the examples shown in the Figures.

The metric, its inverse, and its determinant for this manifold are given by

$$g_{ww} = 1, \quad g_{\theta\theta} = r^2(w), \quad g^{ww} = 1, \quad g^{\theta\theta} = \frac{1}{r^2(w)}, \quad g = r^2(w) \quad (7)$$

For the particular cases of interest to follow, $r(w)$ is symmetric under $w \rightarrow -w$ and monotonic in $|w|$. In any case, the form of the metric leads to

$$\nabla^2 = \frac{1}{g} \left(r(w) \frac{\partial}{\partial w} \left(r(w) \frac{\partial}{\partial w} \right) + \frac{\partial^2}{\partial \theta^2} \right) \quad (8)$$

which is more transparent after changing radial variable to

$$u = \int_0^w \frac{d\varpi}{r(\varpi)} \quad (9)$$

In terms of u and θ it is now easy to find harmonic functions, i.e. solutions of $\nabla^2 h = 0$, since

$$\nabla^2 = \frac{1}{g} \left(\frac{\partial^2}{\partial u^2} + \frac{\partial^2}{\partial \theta^2} \right) \quad (10)$$

¹For example, it is sufficient but not necessary that all the moments of the charge are finite, i.e. $\int r^m \rho(\vec{r}) d^2r < \infty$ for all positive integer m .

For fixed radius, those h which are periodic in θ with period 2π therefore have the form

$$h_0(u) = a + b u \quad \text{and} \quad h_m^\pm(u, \theta) = c_m e^{-mu} e^{\pm im\theta} \quad \text{for any integer } m \geq 0 \quad (11)$$

Note that h_0 is isotropic, i.e. it has no θ dependence. Reverting back to the original variables for the 2D manifold (6), these periodic harmonic functions are given by

$$h_0(w, \theta) = a + b \int_0^w \frac{d\varpi}{r(\varpi)}, \quad h_m^\pm(w, \theta) = c_m e^{\pm im\theta} \exp\left(-m \int_0^w \frac{d\varpi}{r(\varpi)}\right) \quad \text{for any integer } m \geq 0 \quad (12)$$

By using these harmonic functions, it is not difficult to build Green functions for the invariant Laplacian on the manifold, as solutions to

$$\nabla^2 G(w_1, \theta_1; w_2, \theta_2) = -\frac{1}{\sqrt{g}} \delta(w_1 - w_2) \delta(\theta_1 - \theta_2) \quad (13)$$

A Green function symmetric under $(w_1, \theta_1) \leftrightarrow (w_2, \theta_2)$ is given by

$$\begin{aligned} G(w_1, \theta_1; w_2, \theta_2) &= -\frac{1}{4\pi} \left(\int_{w_<}^{w_>} \frac{d\varpi}{r(\varpi)} \right) + \frac{1}{2\pi} \sum_{m=1}^{\infty} \frac{1}{m} e^{-m \int_{w_<}^{w_>} \frac{d\varpi}{r(\varpi)}} \cos(m(\theta_1 - \theta_2)) \\ &= -\frac{1}{4\pi} \left(\int_{w_<}^{w_>} \frac{d\varpi}{r(\varpi)} \right) - \frac{1}{4\pi} \ln \left(1 + e^{-2 \int_{w_<}^{w_>} \frac{d\varpi}{r(\varpi)}} - 2e^{-\int_{w_<}^{w_>} \frac{d\varpi}{r(\varpi)}} \cos(\theta_1 - \theta_2) \right) \end{aligned} \quad (14)$$

where $w_{>,<} = \max, \min(w_1, w_2)$. In the second line of (14), we have summed the Taylor series using

$$\sum_{n=1}^{\infty} \frac{1}{n} z^n \cos(n\theta) = -\frac{1}{2} \ln(1 + z^2 - 2z \cos \theta) \quad (15)$$

$G(w_1, \theta_1; w_2, \theta_2)$ has the usual interpretation as the potential at (w_1, θ_1) due to a point source at (w_2, θ_2) .

If $\int_{w_<}^{w_>} \frac{d\varpi}{r(\varpi)} \rightarrow +\infty$ either as $w_> \rightarrow +\infty$ or as $w_< \rightarrow -\infty$, the Green function (14) satisfies the boundary condition that all the θ -dependent terms vanish as either $w_1 \rightarrow \infty$ for fixed w_2 or as $w_2 \rightarrow -\infty$ for fixed w_1 , leaving only the isotropic term which diverges in either of those limits. However, when $w_2 = 0$ the value of G is not so obvious. Nevertheless, a simple linear combination can be taken to construct a Green function that vanishes at $w_2 = 0$, namely,

$$G_o(w_1, \theta_1; w_2, \theta_2) = G(w_1, \theta_1; w_2, \theta_2) - G(w_1, \theta_1; -w_2, \theta_2) \quad (16)$$

Note that G_o is manifestly an odd function of w_2 and is also an odd function of w_1 as a consequence of $G(w_1, \theta_1; w_2, \theta_2) = G(w_2, \theta_2; w_1, \theta_1)$.

This G_o has a simple interpretation as the potential at (w_1, θ_1) due to a point charge source at (w_2, θ_2) and a negative image charge of that point source at $(-w_2, \theta_2)$. The source and image charges are therefore of *equal* magnitude but opposite sign, and are positioned in an *obvious* way on *opposite* branches of the manifold. So, if both w_1 and w_2 are restricted to one branch of the manifold, (13) will still hold on that branch, since the image will produce an additional Dirac delta only on the other branch. Therefore G_o is an appropriate Green function to solve $\nabla^2 \Phi = -\rho$ on the upper branch of the manifold with the condition $\Phi = 0$ on the inner boundary of that branch, i.e. on the circular ring at $w = 0$.

To verify that G is indeed a solution to (13) two steps are required. Firstly, it is necessary to show $\nabla^2 G = 0$ for non-coincident points on the manifold, but this is guaranteed by the harmonicity of the functions used to build G . Secondly, it is also necessary to show how the Dirac deltas arise.

In regard to this second step, note the discontinuities in the radial derivatives

$$r(w_1) \frac{d}{dw_1} \int_{w_<}^{w_>} \frac{d\varpi}{r(\varpi)} = \Theta(w_1 - w_2) - \Theta(w_2 - w_1) \quad (17)$$

$$r(w_1) \frac{d}{dw_1} \exp\left(-m \int_{w_<}^{w_>} \frac{d\varpi}{r(\varpi)}\right) = -m(\Theta(w_1 - w_2) - \Theta(w_2 - w_1)) \exp\left(-m \int_{w_<}^{w_>} \frac{d\varpi}{r(\varpi)}\right) \quad (18)$$

where the Heaviside step function is $\Theta(z) = 1$ if $z > 0$ or $\Theta(z) = 0$ if $z < 0$, and whose derivative is a Dirac delta, $d\Theta(z)/dz = \delta(z)$. Thus

$$\frac{d}{dw_1} \left(r(w_1) \frac{d}{dw_1} \int_{w_<}^{w_>} \frac{d\varpi}{r(\varpi)} \right) = 2 \delta(w_1 - w_2) \quad (19)$$

$$\frac{d}{dw_1} \left(r(w_1) \frac{d}{dw_1} \exp \left(-m \int_{w_<}^{w_>} \frac{d\varpi}{r(\varpi)} \right) \right) = -2m \delta(w_1 - w_2) + m^2 \exp \left(-m \int_{w_<}^{w_>} \frac{d\varpi}{r(\varpi)} \right) \quad (20)$$

Using these facts, along with

$$\frac{1}{2\pi} \sum_{m=-\infty}^{\infty} e^{im(\theta_1 - \theta_2)} = \delta(\theta_1 - \theta_2) \quad (21)$$

when acting on a space of periodic functions, the Dirac deltas on the RHS of (13) are verified.

p -norm wormholes

Next, consider a class of “ p -norm radial functions” with R a constant radius, $p \geq 1$ a real number, and

$$r(w) = (R^p + |w|^p)^{1/p} \quad (22)$$

Particular cases of the 2D manifolds defined by (22) and (6) are shown in the Figures, as 3D embeddings of surfaces of revolution about the z -axis. For the special case of an Ellis wormhole [5]

$$r(w) = \sqrt{R^2 + w^2} \quad (23)$$

In this special case (14) becomes

$$G(w_1, \theta_1; w_2, \theta_2) = \frac{1}{4\pi} \ln \left[\left(\sqrt{\frac{w_1^2}{R^2} + 1} - \frac{w_1}{R} \right) \left(\sqrt{\frac{w_2^2}{R^2} + 1} + \frac{w_2}{R} \right) \right] \quad (24)$$

$$- \frac{1}{4\pi} \ln \left[1 + \left(\sqrt{\frac{w_1^2}{R^2} + 1} - \frac{w_1}{R} \right)^2 \left(\sqrt{\frac{w_2^2}{R^2} + 1} + \frac{w_2}{R} \right)^2 - 2 \left(\sqrt{\frac{w_1^2}{R^2} + 1} - \frac{w_1}{R} \right) \left(\sqrt{\frac{w_2^2}{R^2} + 1} + \frac{w_2}{R} \right) \cos(\theta_1 - \theta_2) \right]$$

while G_o is the previous linear combination (16).

A contour plot of G versus w_1 and θ_1 is shown in Figure 10, for the Ellis wormhole, with unit source at $(w_2, \theta_2) = (1, 0)$. For comparison, a similar plot of G_o is shown in Figure 11 with the same source as well as its negative image at $(-w_2, \theta_2) = (-1, 0)$.

Squashing the wormhole

Flattening the two branches of the wormhole, to obtain a “two-sided” surface of zero “height” containing a hole of fixed radius R , is achieved by taking the $p = 1$ “Manhattan norm”²

$$r(w) = R + |w| \quad (25)$$

It suffices to consider two cases for the source and field point locations, either with w_1 and w_2 on the same branch of the manifold (i.e. on the same side of the two-sided surface), or with w_1 and w_2 on opposite branches (i.e. on opposite sides of the two-sided surface). Suppose w_1 is always on the upper branch, say. Then the two cases lead to

$$\int_{w_<}^{w_>} \frac{dv}{R + |\nu|} = \ln \left(\frac{R + w_>}{R + w_<} \right) \quad \text{if } w_1 > 0 \text{ and } w_2 > 0 \quad (26)$$

$$\int_{w_<}^{w_>} \frac{dv}{R + |\nu|} = \int_0^{w_1} \frac{dv}{R + v} + \int_{w_2}^0 \frac{dv}{R - v} = \ln \left(\frac{R + w_1}{R} \right) + \ln \left(\frac{R - w_2}{R} \right) \quad \text{if } w_1 > 0 \text{ but } w_2 < 0 \quad (27)$$

²In the opposite extreme, where $p \rightarrow \infty$, the p -norm wormhole becomes the right-circular cylinder of [8], p 488, Eqn (3).

In the first case, with $w_1 > 0$ and $w_2 > 0$, (14) becomes

$$\begin{aligned} G(w_1, \theta_1; w_2, \theta_2)|_{\substack{w_1 > 0 \\ w_2 > 0}} &= -\frac{1}{4\pi} \ln \left[\left(\frac{R+w_>}{R+w_<} \right) \left(1 + \left(\frac{R+w_<}{R+w_>} \right)^2 - 2 \left(\frac{R+w_<}{R+w_>} \right) \cos(\theta_1 - \theta_2) \right) \right] \\ &= -\frac{1}{4\pi} \ln \left(\frac{r_1^2 + r_2^2 - 2r_1 r_2 \cos(\theta_1 - \theta_2)}{r_1 r_2} \right) \end{aligned} \quad (28)$$

where in the second line we have identified $r_1 = R + |w_1|$ and $r_2 = R + |w_2|$, to obtain a symmetrical form that can also be used if $w_1 < 0$ and $w_2 < 0$.

In the second case, with $w_1 > 0$ but $w_2 < 0$, (14) becomes

$$\begin{aligned} G(w_1, \theta_1; w_2, \theta_2)|_{\substack{w_1 > 0 \\ w_2 < 0}} &= -\frac{1}{4\pi} \ln \left[\left(\frac{R+w_1}{R} \frac{R-w_2}{R} \right) \left(1 + \left(\frac{R^2}{(R+w_1)(R-w_2)} \right)^2 - \frac{2R^2}{(R+w_1)(R-w_2)} \cos(\theta_1 - \theta_2) \right) \right] \\ &= -\frac{1}{4\pi} \ln \left(\frac{r_1 r_2}{R^2} + \frac{R^2}{r_1 r_2} - 2 \cos(\theta_1 - \theta_2) \right) \end{aligned} \quad (29)$$

where in the last line we have again identified $r_1 = R + |w_1|$ and $r_2 = R + |w_2|$, to obtain a symmetrical form that can also be used if $w_1 < 0$ and $w_2 > 0$. Taken together, (28) and (29) yield $G(w_1, \theta_1; w_2, \theta_2)$ for any w_1 and w_2 .

A contour plot of G versus w_1 and θ_1 for the squashed wormhole is shown in Figure 12, with unit source at $(w_2, \theta_2) = (1, 0)$.

With these results in hand, it is instructive to compare the result (28) for the squashed wormhole, with its two branches, to the Green function for a single copy of the entire Euclidean plane, (2), at identical points. The difference is given by

$$G(w_1, \theta_1; w_2, \theta_2)|_{\substack{w_1 > 0 \\ w_2 > 0}} - G_{\mathbb{E}_2}(\vec{r}_1; \vec{r}_2) = -\frac{1}{4\pi} \ln \left(\frac{R^2}{r_1 r_2} \right) \quad (30)$$

It is also instructive to compare (29) to (2) when the source point for the latter is interior to the circle of radius R , at a location $\vec{r}_2 = \frac{R^2}{r_2^2} \vec{r}_2$ with $r_2 > R$, so that $r_2 = \frac{R^2}{r_2} < R$. The difference is now given by

$$G(w_1, \theta_1; w_2, \theta_2)|_{\substack{w_1 > 0 \\ w_2 < 0}} - G_{\mathbb{E}_2} \left(\vec{r}_1; \frac{R^2}{r_2^2} \vec{r}_2 \right) = \frac{1}{4\pi} \ln \left(\frac{r_1}{r_2} \right) \quad (31)$$

Note that the terms on the RHS's of (30) and (31) are harmonic on \mathbb{E}_2 so long as $r_1 \neq 0 \neq r_2$, i.e. on the ‘‘punctured plane’’ these terms are harmonic.

Upon taking the linear combination (16), a Green function is obtained for the situation where the circular ring connecting the two flat branches of the squashed manifold is grounded. Explicitly, using (28) and (29), when w_1 and w_2 have the same sign the result is

$$G_o(w_1, \theta_1; w_2, \theta_2) = -\frac{1}{4\pi} \ln \left(\frac{1}{r_1 r_2} (r_1^2 + r_2^2 - 2r_1 r_2 \cos(\theta_1 - \theta_2)) \right) + \frac{1}{4\pi} \ln \left(\frac{r_1 r_2}{R^2} + \frac{R^2}{r_1 r_2} - 2 \cos(\theta_1 - \theta_2) \right) \quad (32)$$

with $r_1 = R + |w_1|$ and $r_2 = R + |w_2|$. When w_1 and w_2 have opposite signs, G_o has an overall sign change because G_o is an odd function of w_1 for fixed w_2 . Combining the various terms then gives the final result for the squashed wormhole grounded on the circle of radius R . When w_1 and w_2 have the same sign,

$$G_o(w_1, \theta_1; w_2, \theta_2) = -\frac{1}{4\pi} \ln \left(R^2 \frac{r_1^2 + r_2^2 - 2r_1 r_2 \cos(\theta_1 - \theta_2)}{r_1^2 r_2^2 + R^4 - 2R^2 r_1 r_2 \cos(\theta_1 - \theta_2)} \right) \quad (33)$$

As a function of \vec{r}_1 and \vec{r}_2 , this is precisely the well-known Green function for points outside a grounded ring on a single copy of the Euclidean plane \mathbb{E}_2 , as obtained by other means. Note that it is symmetric under $(w_1, \theta_1) \leftrightarrow (w_2, \theta_2)$, or equivalently under $\vec{r}_1 \leftrightarrow \vec{r}_2$.

A contour plot of G_o for the squashed wormhole is shown in Figure 13, again with a unit source at $(w_2, \theta_2) = (1, 0)$ as well as its negative image at $(-w_2, \theta_2) = (-1, 0)$.

Curiously, however, there is a subtlety due to a slight disparity between (33) and the Euclidean Green function obtained just by taking the linear combination (LC)

$$G_{\mathbb{E}_2\text{LC}}(\vec{r}_1; \vec{r}_2) = G_{\mathbb{E}_2}(\vec{r}_1; \vec{r}_2) - G_{\mathbb{E}_2}\left(\vec{r}_1; \frac{R^2}{r_2^2} \vec{r}_2\right) \quad (34)$$

This combination can be interpreted as the potential at the field point \vec{r}_1 due to a unit source charge outside the ring, at position \vec{r}_2 , and a negative unit image source inside the ring, at position $\frac{R^2}{r_2^2} \vec{r}_2$. The disparity is given by

$$G_o(w_1, \theta_1; w_2, \theta_2) = G_{\mathbb{E}_2\text{LC}}(\vec{r}_1; \vec{r}_2) - \frac{1}{2\pi} \ln\left(\frac{R}{r_2}\right) \quad (35)$$

and in part it arises because, unlike G_o , the combined $G_{\mathbb{E}_2\text{LC}}$ is *not* symmetric under $\vec{r}_1 \leftrightarrow \vec{r}_2$. But perhaps a better way to understand the disparity is to construct the Green function for a grounded hypersphere in N spatial dimensions and then take the limit as $N \rightarrow 2$ (for example, see [1]). In any case, the additional log term on the RHS of (35) is harmonic on the punctured plane. Consequently, both of the differential equations $\nabla_{r_1}^2 G(\vec{r}_1; \vec{r}_2) = -\delta^2(\vec{r}_1 - \vec{r}_2)$ and $\nabla_{r_2}^2 G(\vec{r}_1; \vec{r}_2) = -\delta^2(\vec{r}_1 - \vec{r}_2)$ will still be satisfied for points \vec{r}_1 and \vec{r}_2 outside the circle of radius R , as will the homogeneous Dirichlet boundary condition for all \vec{r}_2 on the circle, namely, $G(\vec{r}_1; \vec{r}_2)|_{\vec{r}_2=R\hat{r}} = 0$, no matter whether G is taken to be G_o or $G_{\mathbb{E}_2\text{LC}}$.

Relating image charge distributions by inversion

Coordinate inversion on the plane maps the interior of the circular ring to the exterior, and vice versa, and therefore inversion should be expected to relate the standard image method, where the so-called Kelvin image is placed inside the ring, to the Sommerfeld method for the squashed wormhole. Indeed, inversion of the source position is the technique that is normally invoked to locate Kelvin images for grounded sphere Green functions in any dimension.

The inversion mapping is defined by

$$\vec{r} = \frac{R^2}{r^2} \vec{r} \quad (36)$$

Radial distances change under the inversion, $\tau = R^2/r$, but angles do not, $\hat{\tau} = \hat{r}$. Under an inversion the Laplacian does *not* transform into a geometric factor multiplying just the Laplacian, *except in 2D*. In other dimensions, N , the Laplacian mixes with the *scale operator* under an inversion, as follows (for example, see [1]).

$$\nabla_r^2 = \left(\frac{\tau^2}{R^2}\right)^2 \left(\nabla_\tau^2 + \frac{2(2-N)}{\tau^2} D_\tau\right), \quad D_\tau = \vec{\tau} \cdot \vec{\nabla}_\tau \quad (37)$$

This statement may be understood by considering harmonic functions, upon noting that under inversions r effectively becomes $1/r$, and only in 2D do both r^l and r^{-l} appear as factors in harmonic functions. In N dimensions the factors are r^l and r^{2-N-l} .

Moreover, G itself is *not* invariant under the inversion, *except in 2D*. This is obvious on dimensional grounds, since $G(\vec{r}, 0) \propto 1/r^{N-2} \xrightarrow{\text{inversion}} \tau^{N-2}/R^{2N-4} \propto (\tau^{2N-4}/R^{2N-4}) G(\vec{\tau}, 0)$. More precisely, in N spatial dimensions,

$$G(\vec{r}_1; \vec{r}_2) \xrightarrow{\text{inversion}} \frac{\tau_1^{N-2} \tau_2^{N-2}}{R^{2N-4}} G(\vec{\tau}_1; \vec{\tau}_2) \quad (38)$$

Note the symmetry under $\vec{r}_1 \leftrightarrow \vec{r}_2$ is maintained under $\vec{\tau}_1 \leftrightarrow \vec{\tau}_2$. The complete transformation of the differential equation for the Green function in N dimensions is

$$\nabla_{r_1}^2 G(\vec{r}_1; \vec{r}_2) = -\frac{1}{\sqrt{g}} \delta^N(\vec{r}_1 - \vec{r}_2) \xrightarrow{\text{inversion}} \quad (39)$$

$$\left(\frac{\tau_1^2}{R^2}\right)^2 \left(\nabla_{\tau_1}^2 + \frac{2(2-N)}{\tau_1^2} D_{\tau_1}\right) \left(\frac{\tau_1^{N-2} \tau_2^{N-2}}{R^{2N-4}} G(\vec{\tau}_1; \vec{\tau}_2)\right) = -\frac{\tau_1^{N+1}}{R^{2N}} \delta(\tau_1 - \tau_2) \delta^{N-1}(\hat{\tau}_1 - \hat{\tau}_2) \quad (40)$$

Again the 2D case is especially simple. In 2D, up to a common factor, the equation is unchanged in form by the inversion. Thus the following must simultaneously hold in 2D.

$$\nabla_{\vec{r}_1}^2 G(\vec{r}_1; \vec{r}_2) = -\frac{1}{r_1} \delta(r_1 - r_2) \delta(\theta_1 - \theta_2) , \quad \nabla_{\vec{r}_1}^2 G(\vec{r}_1; \vec{r}_2) = -\frac{1}{r_1} \delta(r_1 - r_2) \delta(\theta_1 - \theta_2) \quad (41)$$

In view of these results, it is not difficult to map only the lower branch of the squashed wormhole into the interior of the ring while leaving the upper branch unchanged, thereby obtaining a single copy of 2D Euclidean space that includes both the exterior and the interior of the circle. In the course of this inversion, the image charge is moved to its more conventional position within the ring. We leave the details as an exercise for the reader.

Brief remarks on the grounded conducting disk in 3D

Hobson used Sommerfeld’s method and a clever coordinate choice to find the Green function for an equipotential circular disk in three Euclidean dimensions (3D) [7]. In this approach, the disk serves as a doorway between two copies of 3D Euclidean space, \mathbb{E}_3 , with the unit source and field point located in one copy of \mathbb{E}_3 , and an equal strength, negative image of the source obviously placed in the same position as the source except in the second copy of \mathbb{E}_3 .

Some seventy years later, Davis and Reitz independently solved the same problem, again using Sommerfeld’s method, with an emphasis on the use of complex analysis to construct the Green function [2]. In this regard, their approach is more in line with Sommerfeld’s original analysis, wherein complex variables also play a central role.

Neither of these treatments invoke Riemannian geometry as we have done here for the conducting ring in 2D. However it is possible in principle to consider the conducting disk in 3D as a squashed oblate spheroid, and thereby obtain the Green function for the disk by taking a limit of Green functions on branched manifolds connected by spheroidal generalizations of the Ellis wormhole, analogous to the p -norm wormholes used above. This more geometrical treatment will be discussed elsewhere [1].

Conclusions

We have obtained the Green function for a grounded circular ring in two spatial dimensions by first constructing Green functions on two-dimensional Riemannian manifolds (commonly but rather unfortunately known as “wormholes”) and then by squashing these manifolds to produce two copies of flat Euclidean planes creased together along a circular hole of radius R . The distribution of source and image charges on the final squashed manifold illustrates Sommerfeld’s generalization of Thomson’s method.

Sommerfeld knew that his generalized method could be used to solve a large variety of problems [11], writing to Klein in the spring of 1897 (see [3] page 80):

“The number of boundary value problems solvable by means of my elaborated Thomson’s method of images is very great.”

But he does not seem to have explicitly pursued this during the next half-century, perhaps because more interesting mathematics and physics questions captured his attention.

In our opinion, the most prescient aspect of Sommerfeld’s nineteenth century work lies in its suggestion that physical problems in electromagnetic theory may be simplified and perhaps more easily understood through the study of Riemannian geometries, a view that developed much later in general relativity. However, like Riemann before him, in 1897 Sommerfeld had no reason to include time along with the spatial dimensions of his envisioned manifolds, thus making his work premature.

Nevertheless, considering its application of Riemann’s ideas from geometry and complex analysis to higher dimensional branched manifolds, we believe Sommerfeld’s work should be recognized as a legitimate precursor to the wormhole studies that appeared a few decades later [6, 4, 5] and continue to the present day [10, 8]. We hope our paper encourages readers to share this opinion.

Acknowledgements It has been our pleasure to reconsider this elementary subject during the year of the Feynman Centennial and the Sommerfeld Sesquicentennial. This work was supported in part by a University of Miami Cooper Fellowship, and by a Clark Way Harrison Visiting Professorship at Washington University in Saint Louis.

References

- [1] H M H Alshal and T L Curtright, in preparation.
- [2] L C Davis and J R Reitz, “Solution to potential problems near a conducting semi-infinite sheet or conducting disc” Am. J. Phys. 39 (1971) 1255-1265.
- [3] M Eckert, *Arnold Sommerfeld: Science, Life and Turbulent Times 1868-1951*, Springer-Verlag (2013) ISBN-13: 978-1461474609.
- [4] A Einstein and N Rosen, “The Particle Problem in the General Theory of Relativity” Phys. Rev. 48 (1935) 73-77.
- [5] H G Ellis, “Ether flow through a drainhole: A particle model in general relativity” J. Math. Phys. 14 (1973) 104-118.
- [6] L Flamm, “Beiträge zur Einsteinschen Gravitationstheorie” Physikalische Zeitschrift 17 (1916) 448-454.
- [7] E. W. Hobson, “On Green’s function for a circular disc, with application to electrostatic problems” Trans. Cambridge Philos. Soc. 18 (1900) 277- 291.
- [8] O James, E von Tunzelmann, P Franklin, and K S Thorne, “Visualizing *Interstellar’s* Wormhole” Am. J. Phys. 83 (2015) 486-499 [<https://arxiv.org/abs/1502.03809>].
- [9] J Mehra, *The Beat of a Different Drum: The Life and Science of Richard Feynman*, Oxford University Press (1994) ISBN-13: 978-0198539483.
- [10] M S Morris and K S Thorne, “Wormholes in spacetime and their use for interstellar travel: A tool for teaching general relativity” Am. J. Phys. 56 (1988) 395-412.
- [11] A Sommerfeld, “Über verzweigte Potentiale im Raum” Proc. London Math. Soc. (1896) s1-28 (1): 395-429.

Figures

The first nine Figures show 3D embeddings of various 2D p -norm wormholes, where

$$(ds)^2 = (dw)^2 + r^2(w) (d\theta)^2 = (dx)^2 + (dy)^2 + (dz)^2 \quad (\text{F1})$$

$$x(w, \theta) = r(w) \cos \theta, \quad y(w, \theta) = r(w) \sin \theta, \quad r(w) = \left(R^p + (w^2)^{p/2} \right)^{1/p} \quad (\text{F2})$$

$$z(w) = \int_0^w \sqrt{1 - (dr(\varpi)/d\varpi)^2} d\varpi = \int_0^w \sqrt{1 - (\varpi^2)^{p-1} \left(R^p + (\varpi^2)^{p/2} \right)^{\frac{2}{p}-2}} d\varpi \quad (\text{F3})$$

For example, for $p = 2$,

$$z(w) = R \ln \left(\frac{w + \sqrt{R^2 + w^2}}{R} \right) = R \operatorname{arcsinh} \left(\frac{w}{R} \right) \quad (\text{F4})$$

For generic p , it is easiest to obtain $z(w)$ by numerical solution of

$$\frac{dz(w)}{dw} = \sqrt{1 - (w^2)^{p-1} \left(R^p + (w^2)^{p/2} \right)^{\frac{2}{p}-2}} \quad (\text{F5})$$

with initial condition $z(0) = 0$.

Figures 1-9: Embedded surfaces for p -norm wormholes, where $p = 1 + 1/2^k$, $k = 0, 1, 2, 3, 4, 5, 6, 7, 8$. All plots are in units where $R = 1$, with $0 \leq \theta \leq 2\pi$ and $-2 \leq w \leq 2$. Upper and lower branches of the surfaces are shown in orange and green, respectively.

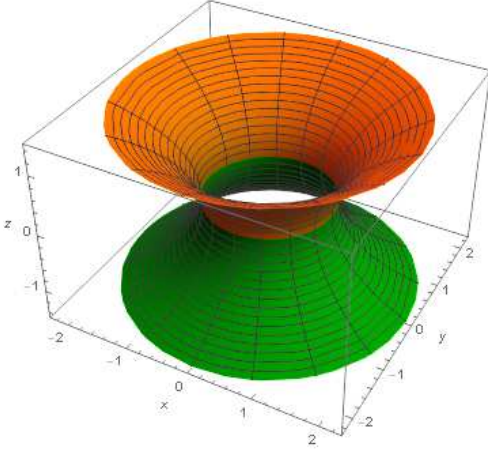


Figure 1: $p = 2$

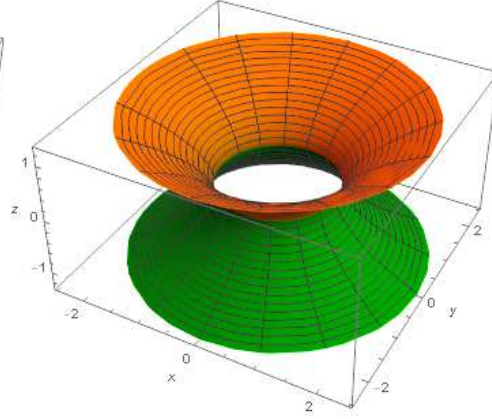


Figure 2: $p = 3/2$

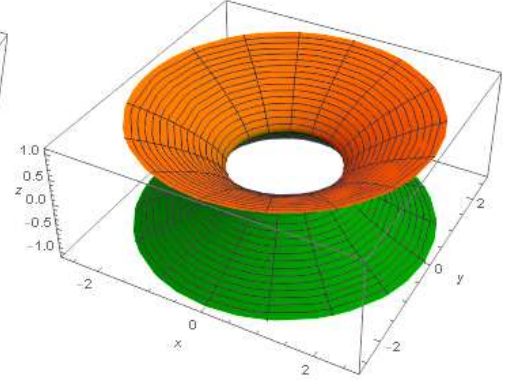


Figure 3: $p = 5/4$

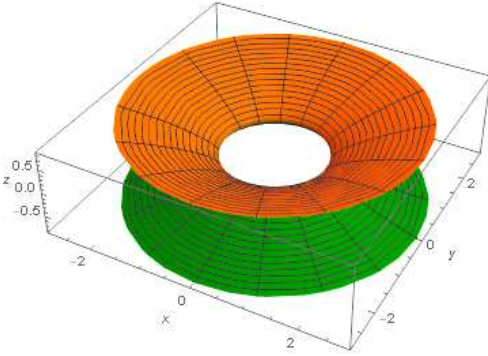


Figure 4: $p = 9/8$

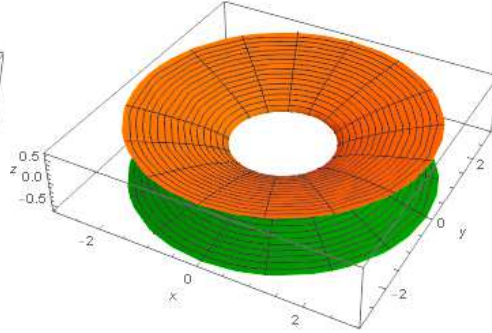


Figure 5: $p = 17/16$

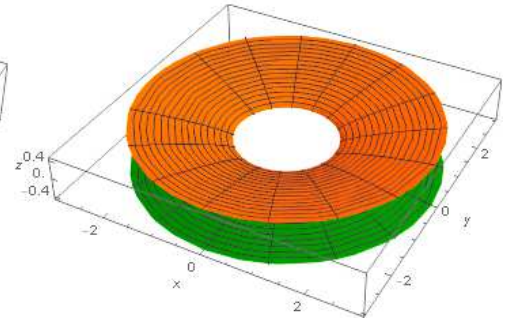


Figure 6: $p = 33/32$

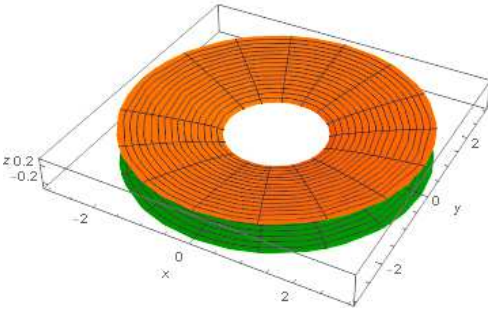


Figure 7: $p = 65/64$

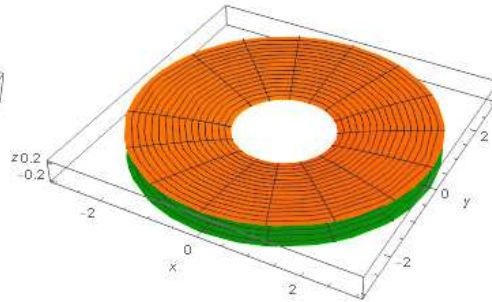


Figure 8: $p = 129/128$

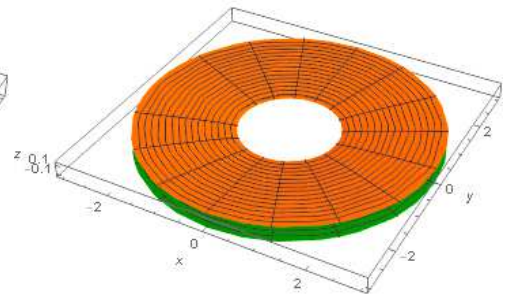


Figure 9: $p = 257/256$

The next four Figures show contour plots of various Green functions, with $-\pi \leq \theta_1 \leq \pi$ along the vertical axes, and $-5 \leq w_1 \leq 5$ along the horizontal axes.

Figure 10: A plot of (24) with source at $(w_2, \theta_2) = (1, 0)$.

Figure 11: A plot of (16) using (24) with source at $(w_2, \theta_2) = (1, 0)$ & image at $(-w_2, \theta_2) = (-1, 0)$.

Figure 12: A plot of (28) and (29) with source at $(w_2, \theta_2) = (1, 0)$.

Figure 13: A plot of (33), correctly signed, with source at $(w_2, \theta_2) = (1, 0)$ & image at $(-w_2, \theta_2) = (-1, 0)$.

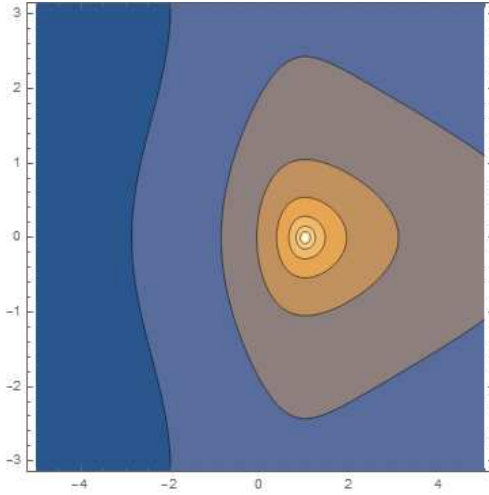


Figure 10: Contour plot of G for the Ellis wormhole.

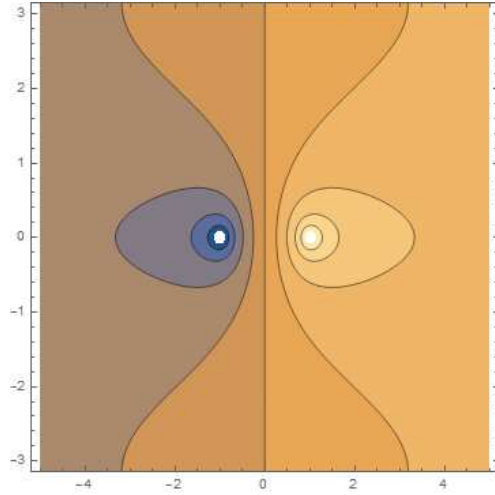


Figure 11: Contour plot of G_o for the Ellis wormhole.

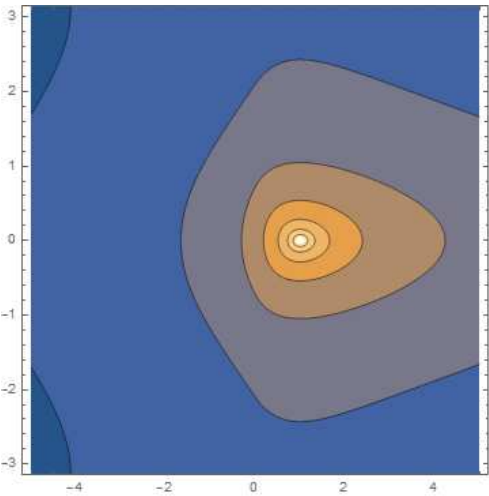


Figure 12: Contour plot of G for the squashed wormhole.

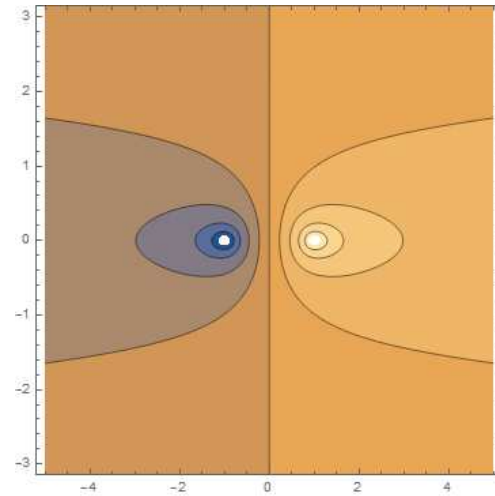


Figure 13: Contour plot of G_o for the squashed wormhole.